

4. FUSION-PRODUCT LOSSES TO FIRST WALL

The fraction of particles lost to the wall from a given birth point is:

$$f_{\ell} = \frac{\int_{\cos\chi_{\max}}^{\cos\chi_{\min}} 2\pi d(\cos\chi)}{\int_{-1}^1 2\pi d(\cos\chi)} \frac{1}{2}(\cos\chi_{\min} - \cos\chi_{\max}). \quad (4.1)$$

The trapping fraction can be calculated as an immediate consequence of (4.1). For a birth point having zero loss region, the first trapped orbit occurs for $\chi = 90^\circ$ and the last for the fattest banana. From (4.1), these conditions determine the trapping fraction:

$$f_T = -\frac{1}{2} \cos\chi_S, \quad (4.2)$$

where $\cos\chi_S$ corresponds to the stagnation orbit, defined by (3.3)-(3.5). When a birth point has a non-zero loss region, the overlap between $\chi_{\min} < \chi < \chi_{\max}$ and $90^\circ < \chi < \chi_S$ must be excluded from f_T . The more general form for f_T is then:

$$f_T = \begin{cases} 0, & \text{for } \chi_{\min} \leq 90^\circ < \chi_S \leq \chi_{\max} & (4.3a) \\ -\frac{1}{2} \cos\chi_{\min}, & \text{for } 90^\circ < \chi_{\min} \leq \chi_S \leq \chi_{\max} & (4.3b) \\ -\frac{1}{2} \cos\chi_S, & \text{for } f_{\ell} = 0, \text{ or } 90^\circ < \chi_S \leq \chi_{\min} < \chi_{\max} & (4.3c) \end{cases}$$

Figs. 2.3a-c illustrate (4.3a) and Figs. 2.2b-2.2c illustrate (4.3b).

The net loss fraction is:

$$F_{\ell} = \frac{\text{total fusion products lost from plasma}}{\text{total fusion products produced}}$$

$$= \int_V f_{\ell} n_1 n_2 \langle \sigma v \rangle_{12} R r dr d\theta d\phi \bigg/ \int_V n_1 n_2 \langle \sigma v \rangle_{12} R r dr d\theta d\phi. \quad (4.4)$$

This work assumes only Maxwellian fusions [32] with particle density profiles of the form $n = n_0 [1 - \gamma_N (r/a)^L]^K$ and background temperature profiles like $T = T_0 [1 - \gamma_T (r/a)^Q]^P$. Loss fraction results discussed below assume no fusion product scrape-off by a limiter. When losses to the limiter dominate, the limiter position can be used to define the wall; this has been done for example, in our calculations for ORNL-EPR (see Table 2.1).

4.1 Wall Loading Profile

Another important result of this analysis is the wall loading profile i.e. the incident fusion product flux, $\dot{d}n/dA$, as a function of poloidal angle (calculated in units of $\#/m^2\text{-s}$):

$$F \equiv \frac{\dot{d}n}{dA} = \frac{\text{total fusion products lost to the wall between } \theta' \text{ and } \theta'+d\theta'}{\text{toroidal wall area between } \theta' \text{ and } \theta'+d\theta'}$$

$$= \int_V n_1 n_2 \langle \sigma v \rangle_{12} f_{\ell}(r, \theta, \theta') R r dr d\theta d\phi \bigg/ \int_S R r d\theta d\phi, \quad (4.5)$$

where $f_{\ell}(r, \theta, \theta')$ is the loss fraction from a birth point at (r, θ) to a wall position between θ' and $\theta'+d\theta'$. Both (4.4) and (4.5) have been

evaluated numerically, and in particular (4.5) has been computed for equal intervals around the wall, i.e. between θ'_k to θ'_{k+1} , as indicated in Fig. 2.1. Finite gyroradius motion causes the fusion product to be deposited at a minimum distance r_g from the guiding center-wall intersection, with a random phase. The resulting wall loading is strongly smoothed. It is therefore appropriate to choose $\Delta\theta' = \theta'_{k+1} - \theta'_k$ so that $r_w \Delta\theta' = 2 r_g$. A second effect to be considered here is that all the losses occur in the direction of the vertical drift due to ∇B and curvature. Consequently, the losses occur only to the upper- or only to the lower-half plane of the tokamak. The denominator of (4.5) can be evaluated analytically for a strip of area around the torus:

$$\Delta S(\theta'_k, \theta'_{k+1}) = 2\pi [r_w^2 (\sin\theta'_{k+1} - \sin\theta'_k) + R_o r_w (\theta'_{k+1} - \theta'_k)] \quad (4.6)$$

The loss fraction in (4.5) is computed as $f_\ell(r, \theta, \theta'_k \rightarrow \theta'_{k+1})$ using (4.1) where $\cos\chi_{\min}$ and $\cos\chi_{\max}$ correspond to wall-orbit intersections at θ'_k and θ'_{k+1} as calculated from (3.1). Only first bounce (prompt) losses are considered here; wall bombardment due to fusion products that pitch-angle scatter into the loss region during slowing down, not included here, must ultimately be considered. Rough estimates are that pitch-angle losses are as much as an order of magnitude lower than prompt losses. On the other hand, anomalous effects such as shear-Alfven-wave-induced fast ion losses, analyzed by Chan and Sigmar [33], could cause significant localized effects. For this

case, particles pitch-angle scatter by increasing the maximum poloidal radius of the drift orbit, r_{\max} , and thus tend to preferentially bombard the wall in the mid-plane.

4.2 Results

Wall loading profiles for 3.52-MeV alpha losses from PLT, TFTR, ORNL-EPR and UWMAK I (see Table 2.1 for machine parameters) are shown in Fig. 4.1. See Table 4.1 for a summary of the results for each curve (the peak-to-average flux ratio is designated as P/A and the average flux is given as \bar{F}). In PLT and TFTR I, loss contributions occur over the entire plasma. For the larger plasmas, there are successively larger zero-loss, core regions. In TFTR II, the outer 55% of the plasma contributes to wall loading, dropping to 30%

Table 4.1: Summary of 3.52-MeV Alpha Losses for Figure 4.1

Machine	Curve 1 TFTR I	Curve 2 ORNL-EPR	Curve 3 TFTR II	Curve 4 PLT	Curve 5 UWMAK I
F_{ℓ}	0.13	3.1×10^{-3}	0.014	0.48	1.4×10^{-4}
P/A	1.9	1.8	1.4	1.4	2.3
\bar{F}	4.5×10^{15}	1.5×10^{15}	1.1×10^{15}	1.1×10^{15}	1.6×10^{14}

for ORNL-EPR, and to 4% for UWMAK I. This is as expected, since the poloidal gyroradius is comparable to r_w in PLT and TFTR I, less than r_w in TFTR II, and much less than r_w in ORNL-EPR and UWMAK I. Also, note that PLT can be used to simulate TFTR II losses for poloidal wall angles below 135° .

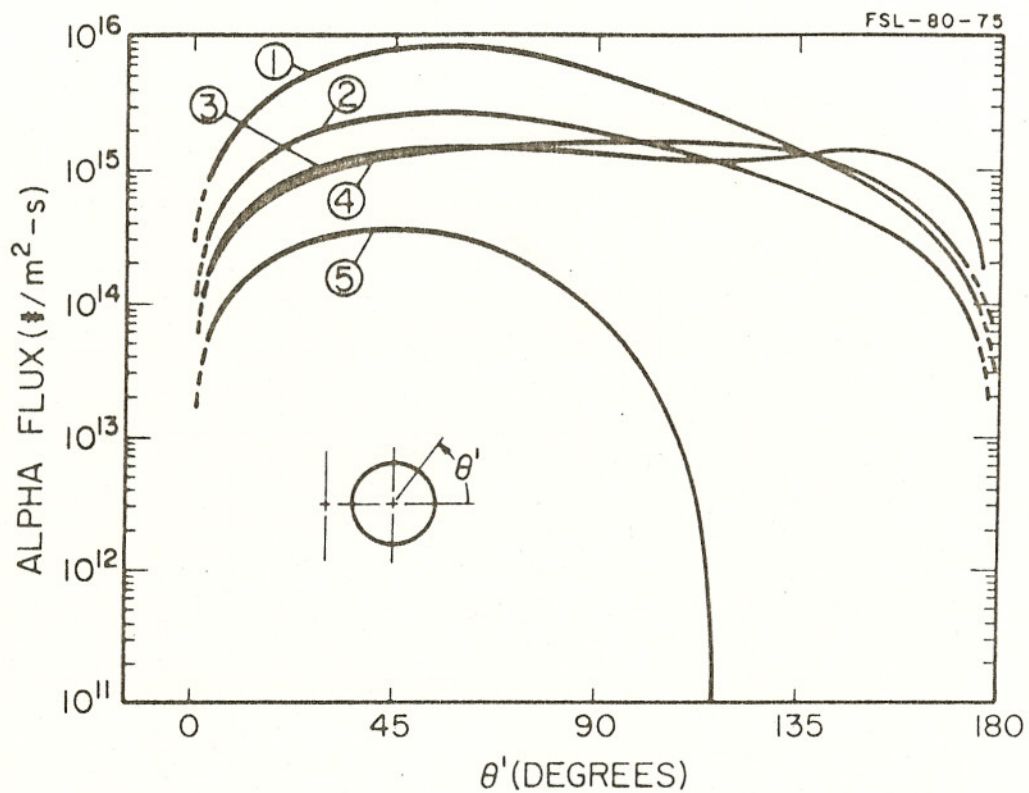


Figure 4.1 Flux of 3.52 MeV alphas on the first wall versus poloidal angle for several representative tokamaks. The loss fraction, F_{ℓ} , peak-to-average flux ratio, P/A , and average flux, F (#/m²-sec), are summarized in Table 4.1.

Losses for various fusion products in PLT are shown in Fig. 4.2. Here, the normalized flux is obtained by dividing the particle flux by the total-fusions-per-second, S , for the given reaction, i.e., the denominator of (4.4). See Table 4.2 for the Figure key. The curves for 3.7-MeV and 3.52-MeV alphas, 3.03-MeV p, and 1.01-MeV T are essentially identical because (2.9) is exact for the last two cases and approximately true for all four. The 14.7-MeV p is poorly confined because the poloidal gyroradius is larger than r_w , while the 0.82-MeV He^3 is well confined because its poloidal gyroradius is much smaller than r_w . Similar results are obtained for various fusion products in the other tokamak machines.

Table 4.2: Summary of Fusion-Product Losses for Figure 4.2

Curve	Fusion-Product	F_ℓ	P/A	\bar{F}	S	
1	D(He^3, p) He^4	14.70 MeV p	0.99	1.6	9.1×10^{11}	1.1×10^{13}
2	D(t, n) He^4	3.52 MeV He^4	0.48	1.4	1.1×10^{15}	2.9×10^{16}
3	D(He^3, p) He^4	3.70 MeV He^4	0.46	1.4	4.3×10^{11}	1.2×10^{13}
4	D(d, p)T	{ 3.03 MeV p 1.01 MeV T	0.44	1.5	1.5×10^{13}	4.2×10^{14}
5	D(d, n) He^3	0.82 MeV He^3	0.07	1.8	2.2×10^{12}	4.2×10^{14}

The wall loading profiles are also strongly influenced by profiles of n , T and J . This profile dependence is strongest in a plasma that has no zero-loss core, i.e., when the fusion product losses are a function of the complete spatial profile. Plasmas having the largest

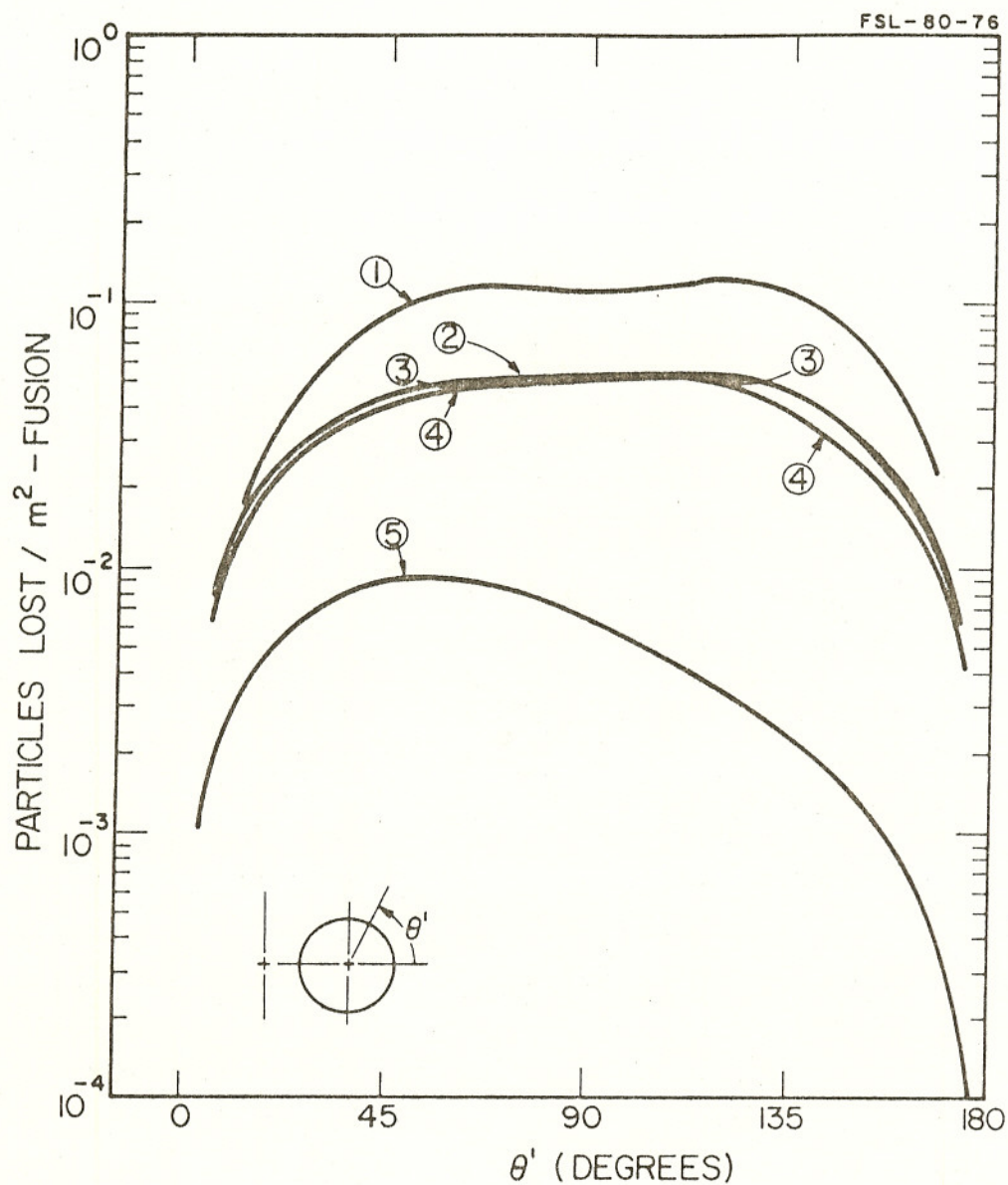


Figure 4.2 Normalized fusion product wall flux for DT, DD and D-He³ reactions in PLT versus poloidal angle. The loss-fraction, F_l , peak-to-average flux ratio, P/A, average flux, \bar{F} (#/m²-sec), and total fusions, S (#/sec), are summarized for each curve in Table 4.2.

zero loss core show the least variation in wall loading as the spatial profiles are changed. Examples of the former case are TFTR I and PLT; UWMAK I is an example of the latter.

4.2.1 Variation with T_i -Profile

Figure 4.3 illustrates the effect of varying the T-profile in TFTR I, from $T/T_0 = 1$, to $T/T_0 = 1 - .8(r/a)$. The peak alpha flux values vary by a factor of 3.7 over this range of T-profiles. The constant-T curve produces the highest overall wall loading because the fusion reactivity is constant over the whole plasma, causing the highest fusion rate. The linear-T profile concentrates fusions at the plasma core, producing the lowest net fusion rate, and consequently the lowest wall loading values. The position of the flux peaks varies only slightly, from $\theta' = 58^\circ$ for $T/T_0 = 1$, to $\theta' = 52^\circ$ for the linear-T plot. The flux peak is shifted to a lower θ' , for a more centrally peaked profile, because losses from the plasma core are concentrated at the outboard portion ($R > R_0$) of the wall. Fusion products born in the plasma fringe move along orbits which hit the wall over a broad range of poloidal angles (compare Fig. 2.2a and 2.2c). Flatter T-profiles enhance these fringe losses, thus broadening the wall loading curve and shifting the peak flux to higher θ' .

4.2.2 Variation with n_i -Profile

The wall bombardment in TFTR I has been calculated for various n-profiles, ranging from $n/n_0 = 1$ to $n/n_0 = 1 - (r/a)$. The resulting alpha flux curves for $n/n_0 = 1 - (r/a)^L$ are essentially identical to the

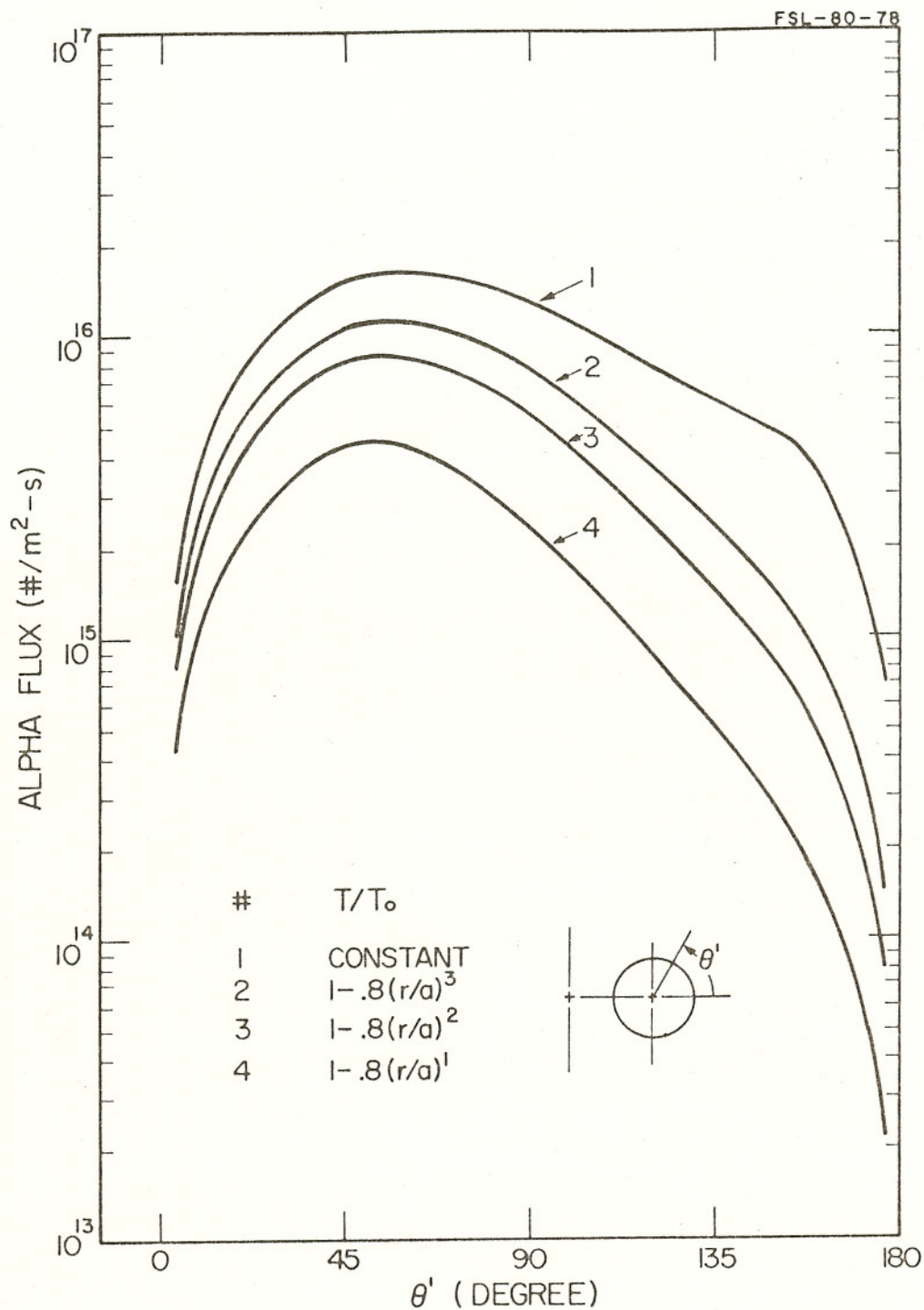


Figure 4.3 Wall loading flux (3.52-MeV α) in TFTR-I versus poloidal wall angle, for various T-profiles. The n- and J-profiles are as given in Table 2.1.

corresponding flux curves (within 10%) for $T/T_0 = 1 - .8(r/a)^Q$. The peak fluxes (F_{pk}) vary by a factor of 3.4 in this case, with the position of these peaks (in θ') identical to the corresponding T-profile flux peaks. This near superposition of wall loading curves occurs because the fusion source rate changes in the same way as the T- and n- profiles are varied.

4.2.3 Variation with Current Profile

Figure 4.4 shows alpha wall loading dependence on J-profile in TFTR I. The extremes in profile are $J/J_0 = 1$, and $J/J_0 = 1 - (r/a)^{.01}$ which is very peaked about $r = 0$; between these two limits, peak fluxes vary by a factor of 2.7. The peaked-J profile produces the largest B_θ at a given poloidal radius (c.f. eqns. 2.4-2.5), yielding the best fusion product confinement, i.e. lowest wall loading. The maximum flux position is strongly dependent on J-profile, decreasing by 40° as $J(r)$ progresses from a constant to very localized at $r = 0$. The constant-J enhances losses from the plasma edges so that the alpha flux curve is flatter and has a maximum for larger θ' . The peaked-J de-emphasizes the fringe losses, shifting the maximum flux position to smaller θ' .

4.2.4 Variations with Geometric Parameters

Geometric factors also are a strong factor in fusion-product loss curves. The variables to be considered are R_0 , a , r_w and $q(a)$. Since wall loading sensitivity to these parameters is stronger in larger machines the example used here is ORNL-EPR.

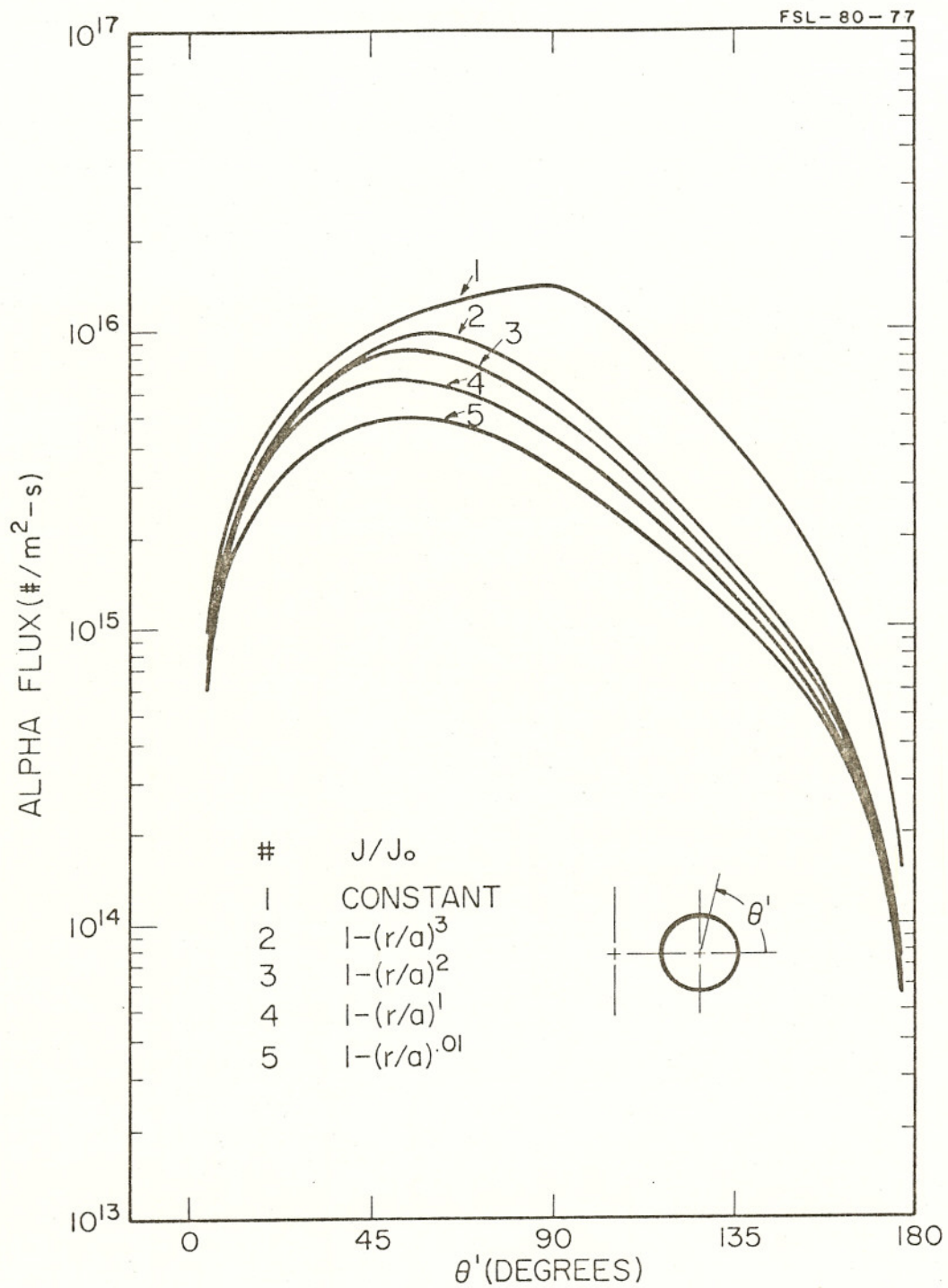


Figure 4.4 Wall loading flux (3.52-MeV α) in TFTR-I versus poloidal wall angle, for various J-profiles. The T- and n-profiles are as given in Table 2.1.

Figure 4.5 is a plot of alpha wall loading in ORNL-EPR for various q -values, ranging from 1.5 to 3.5, resulting in a maximum flux variation by a factor of 32. This very strong flux dependence on q arises because the banana width is proportional to q . The maximum flux position increases slightly with increasing q ($\theta' = 42^\circ$ for $q = 1.5$, $\theta' = 50^\circ$ for $q = 3.5$) because the poorer confinement increases losses for $r \sim a$. This same effect also flattens the wall loading curve somewhat for higher q -values.

The effect of varying r_w is shown in Fig. 4.6 for ORNL-EPR. As the wall radius is increased from nominal ($r_w = a$) to $r_w = 1.3a$, the maximum flux decreases by a factor of 1/4300. This huge variation arises because fewer of the alphas can reach the wall as r_w increases, i.e. the zero-loss core grows from 55% to 80% of the plasma volume. As the zero-loss core increases, the lossy region becomes concentrated in a new-moon shaped sliver at the outboard plasma edge. Consequently, losses are increasingly peaked at lower values of θ' .

Figure 4.7 illustrates the influence of minor radius variations on wall loading in ORNL-EPR. As the minor radius increases from 100 cm to 350 cm, the peak flux decreases by 2 orders of magnitude. This strong dependence results from the zero-loss region increasing from 0 to 70% of the plasma volume as the minor radius increases by a factor of 3.5. Large fusion rates in the plasma core easily outweigh the smaller plasma volume for small minor radii, yielding large alpha wall fluxes. For larger a -values, the combination of a large zero-loss core and low fusion rates in the lossy fringe produce the low wall

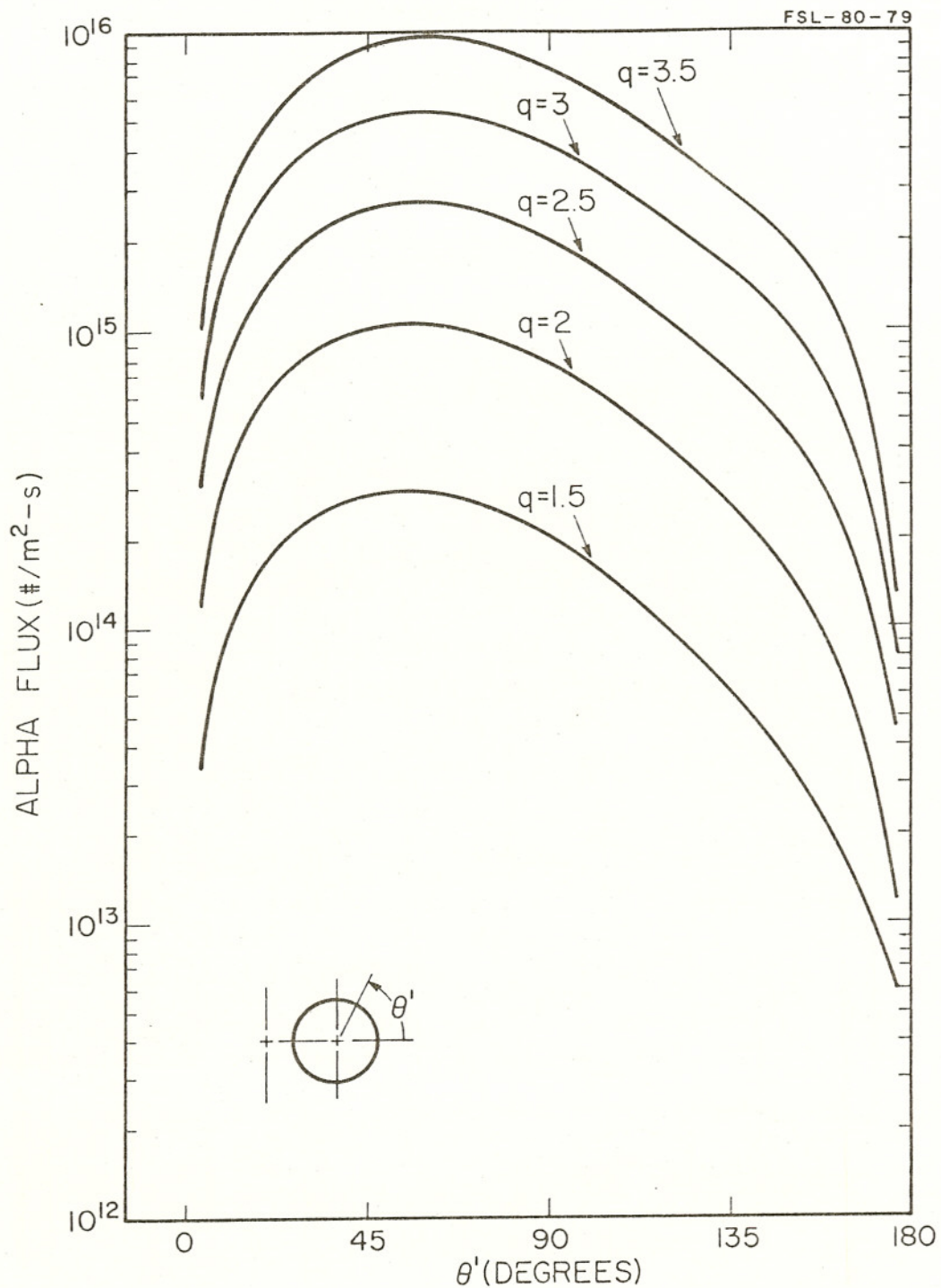


Figure 4.5 Wall loading flux (3.52-MeV α) in ORNL-EPR versus poloidal wall angle, for various q -values. Other parameters are as given in Table 2.1, while I varies consistently with changing q .

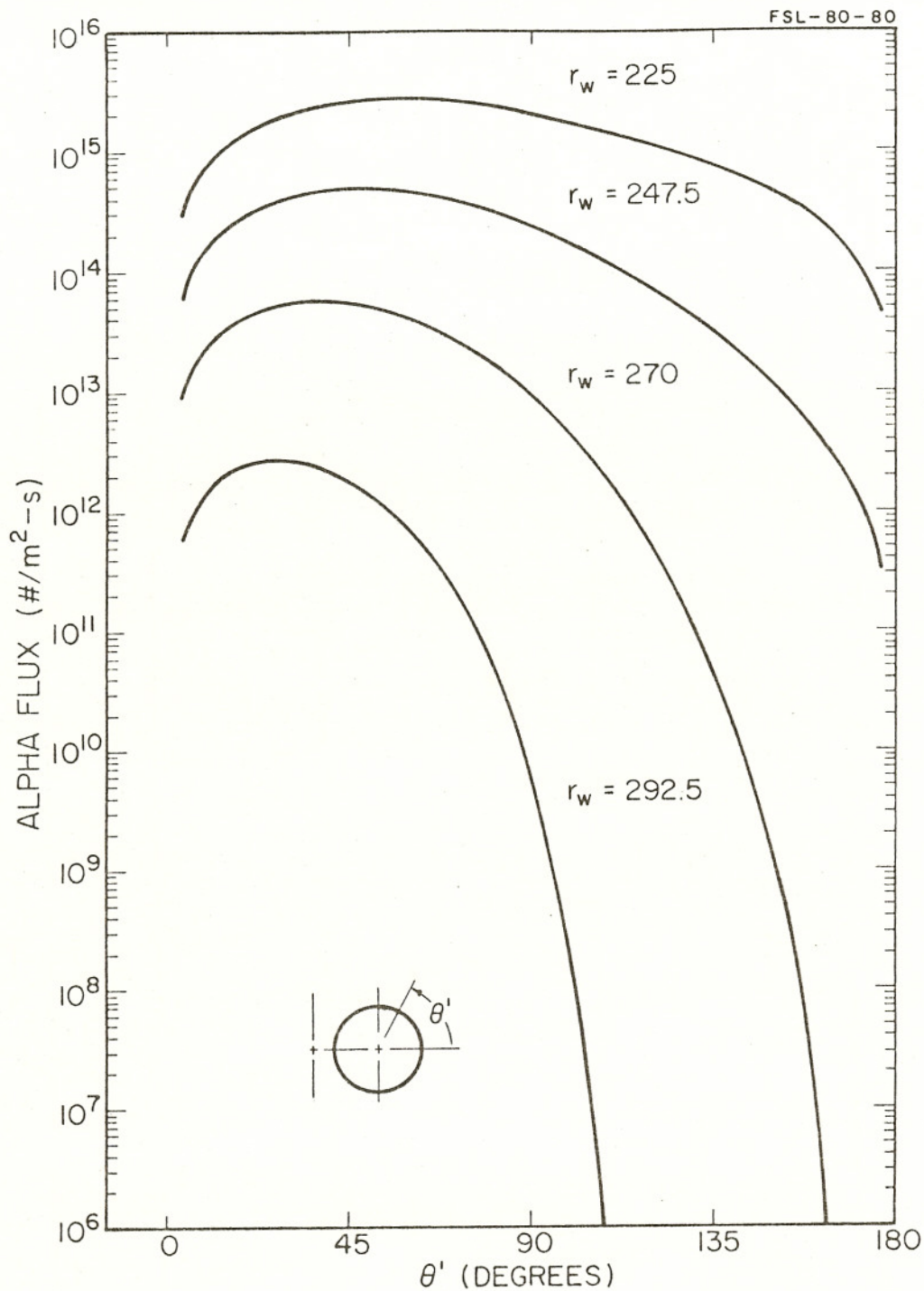


Figure 4.6 Wall loading flux (3.52-MeV α) in ORNL-EPR versus poloidal wall angle, for various values of r_w . All other parameters are as given in Table 2.1.

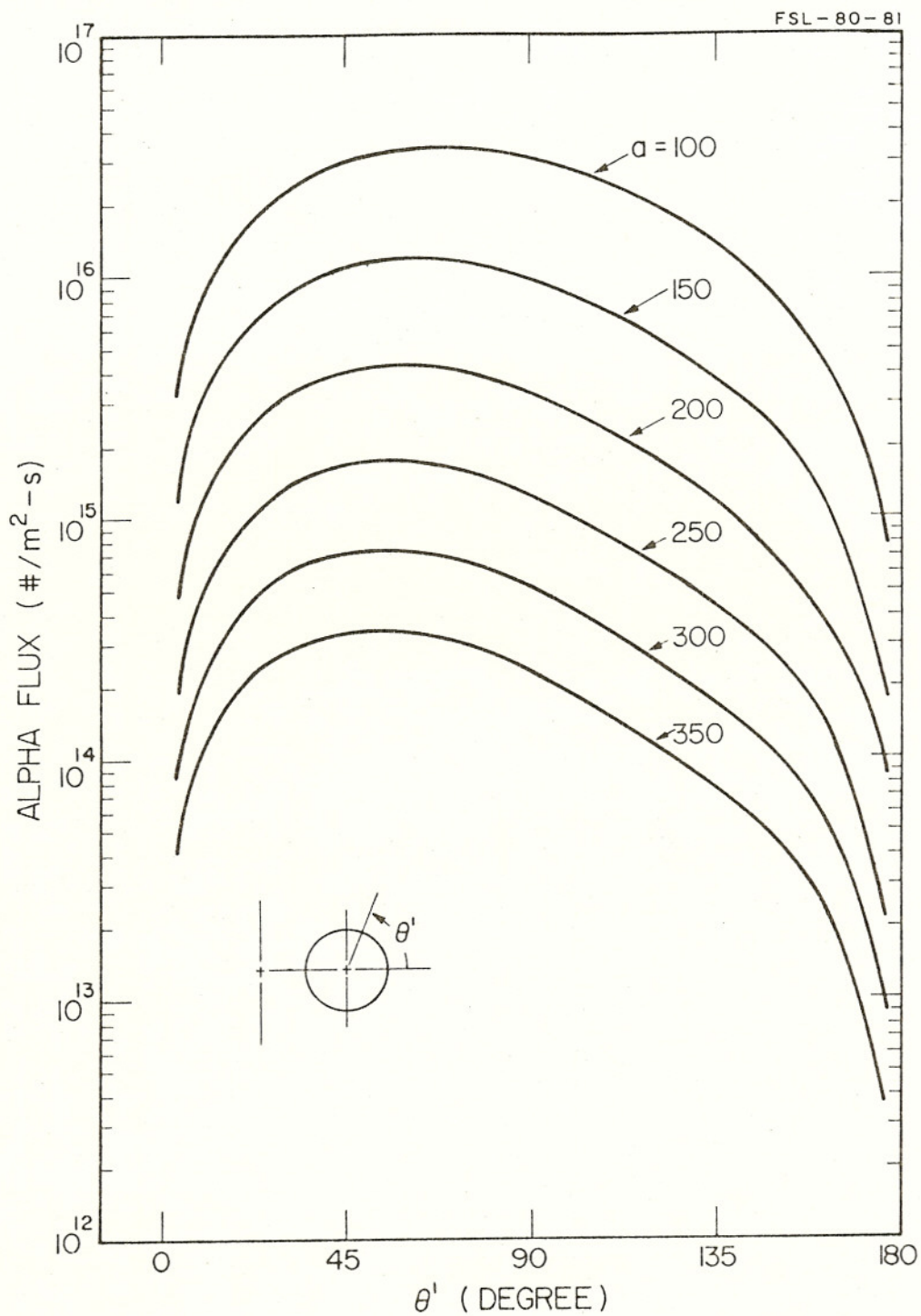


Figure 4.7 Wall loading flux (3.52-MeV α) in ORNL-EPR versus poloidal wall angle, for various values of minor radius. Other parameters are as shown in Table 2.1 while I varies consistently with $q=\text{constant}$.

loadings. The position of maximum flux, θ' , decreases with increasing minor radius because the new moon-shaped, lossy plasma fringe concentrates losses toward the outboard edge.

Figure 4.8 demonstrates the change in normalized wall flux (particle flux divided by total-fusions-per-second, as in Fig. 4.2) as the major radius of ORNL-EPR is varied. This form of the plot was chosen because the curves coalesce. That is, peak flux is roughly proportional to the plasma volume ($4\pi^2 R_0 a^2$); so, increasing R_0 by a factor of 3.1 causes F_{pk} to increase by a factor of 3.6. The additional increase in maximum flux is caused by a decrease in the size of the zero-loss core region as R_0 increases. The zero-loss core size decreases as R_0 is increased because total current is inversely proportional to R_0 for q fixed. The peak flux position is essentially constant as R_0 changes. Coalescence of normalized flux curves does not occur in Fig. 4.7 because the peak flux rapidly decreases for increasing minor radius (see also Table 4.3).

Table 4.3: Summary of 3.52-MeV Alpha Losses for Figure 4.8

R_0	$F_{\ell} \times 10^3$	$F_{pk} \times 10^{-15}$	$\bar{F} \times 10^{-15}$	P/A	$S \times 10^{-20}$
350	1.6	1.3	0.80	1.6	0.77
1100	5.3	4.7	2.6	1.8	2.4

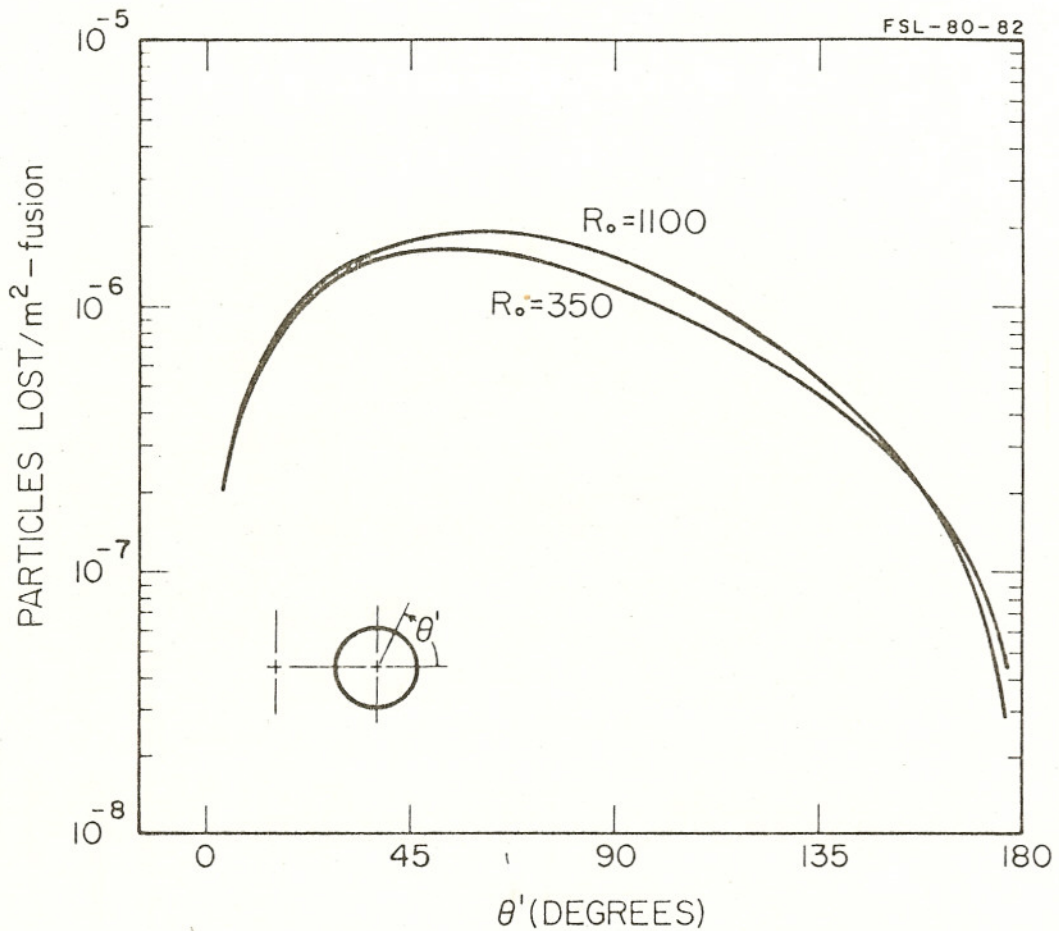


Figure 4.8 Normalized wall loading flux (3.52-MeV α) in ORNL-EPR versus poloidal wall angle, for various values of major radius. Other parameters are as given in Table 2.1, while I varies consistently with q =constant. The loss fraction, F_{ℓ} , peak-to-average flux ratio, P/A , average flux, \bar{F} (#/m²-sec) and total fusions (#/sec) are summarized for each curve in Table 4.2.